

Article

Prediction of Second Melting Temperatures Already Observed in Pure Elements by Molecular Dynamics Simulations

Robert F. Tournier ^{1,*}  and Michael I. Ojovan ^{2,3} 

¹ UPR 3228 Centre National de la Recherche Scientifique, Laboratoire National des Champs Magnétiques Intenses, European Magnetic Field Laboratory, Institut National des Sciences Appliquées de Toulouse, Université Grenoble Alpes, F-31400 Toulouse, France

² Department of Materials, Imperial College London, London SW7 2AZ, UK; m.ojovan@imperial.ac.uk

³ Department of Radiochemistry, Moscow State University, 119991 Moscow, Russia

* Correspondence: robert.tournier@lncmi.cnrs.fr

Abstract: A second melting temperature occurs at a temperature T_{n+} higher than T_m in glass-forming melts after heating them from their glassy state. The melting entropy is reduced or increased depending on the thermal history and on the presence of antibonds or bonds up to T_{n+} . Recent MD simulations show full melting at $T_{n+} = 1.119T_m$ for Zr, $1.126T_m$ for Ag, $1.219T_m$ for Fe and $1.354T_m$ for Cu. The non-classical homogeneous nucleation model applied to liquid elements is based on the increase of the Lindemann coefficient with the heating rate. The glass transition at T_g and the nucleation temperatures T_{nG} of glacial phases are successfully predicted below and above T_m . The glass transition temperature T_g increases with the heating rate up to T_{n+} . Melting and crystallization of glacial phases occur with entropy and enthalpy reductions. A universal law relating T_{n+} and T_{nG} around T_m shows that T_{nG} cannot be higher than $1.293T_m$ for $T_{n+} = 1.47T_m$. The enthalpies and entropies of glacial phases have singular values, corresponding to the increase of percolation thresholds with T_g and T_{nG} above the Scher and Zallen invariant at various heating and cooling rates. The G-phases are metastable up to T_{n+} because the antibonds are broken by homogeneous nucleation of bonds.

Keywords: melting enthalpy and entropy; second melting temperature; melting entropy reduction; crystallization enthalpy reduction; undercooling; overheating; homogeneous nucleation; glasses; liquid–liquid transitions



Citation: Tournier, R.F.; Ojovan, M.I. Prediction of Second Melting Temperatures Already Observed in Pure Elements by Molecular Dynamics Simulations. *Materials* **2021**, *14*, 6509. <https://doi.org/10.3390/ma14216509>

Academic Editor:
Ravichandar Babarao

Received: 23 September 2021
Accepted: 26 October 2021
Published: 29 October 2021

Publisher's Note: MDPI stays neutral with regard to jurisdictional claims in published maps and institutional affiliations.



Copyright: © 2021 by the authors. Licensee MDPI, Basel, Switzerland. This article is an open access article distributed under the terms and conditions of the Creative Commons Attribution (CC BY) license (<https://creativecommons.org/licenses/by/4.0/>).

1. Introduction

Glass transition temperatures are observed at a temperature $T = T_g$ during heating of quenched melts. Below T_g , atomic bonds system produces enthalpy relaxation between the two homogeneous nucleation temperatures T_{n-} of the glassy phase with the highest being T_g [1,2]. The glass formation at the lowest T_{n-} occurs in hyperquenched glass-forming melts at the departure of the enthalpy relaxation [3–6]. Heating the glass through T_g breaks the atomic bonds and gives rise to configurations that are always accompanied by a second-order phase transition [7–12]. The non-classical homogeneous nucleation (NCHM) model predicts the temperatures of glasses, stable and ultrastable glasses [13–25], and glacial phases [26–35] showing that a new phase called Phase 3 appears after heating the quenched liquids through T_g with an enthalpy equal to the difference $\Delta\epsilon_{1g}$ between those of liquids 1 and 2. Quenched Liquid 1 has an initial enthalpy, before giving rise to the glass state, equal to $\epsilon_{1s} H_m$, varying with the square of the reduced temperature $\theta = (T - T_m)/T_m$ as shown in Equation (1) (H_m being the melting heat of crystals) [36]:

$$\epsilon_{1s}(\theta) = \epsilon_{1s0} \left(1 - \theta^2 \times \theta_{0m}^{-2} \right) \quad (1)$$

Liquid 2 has an enthalpy equal to $\varepsilon_{gs} H_m$ in Equation (2):

$$\varepsilon_{gs}(\theta) = \varepsilon_{gs0} \left(1 - \theta^2 \times \theta_{0g}^{-2} \right) + \Delta\varepsilon \quad (2)$$

The reduced temperatures θ_{0m} and θ_{0g} are the Vogel–Fulcher–Tammann temperatures of these two liquids and are defined by the coefficients ε_{ls0} and ε_{gs0} , depending on the nucleation temperatures in the two liquids equal to $[\varepsilon_{ls}(\theta) - 2]/3$ for $\Delta\varepsilon = 0$ [1,36]. The reduced glass transition temperature θ_g is used to define them [37–39]. The coefficient $\Delta\varepsilon$ only intervenes in the enthalpy of quenched liquids, stable and ultrastable glasses and glacial phases. The melting enthalpy and entropy are H_m and S_m at the melting temperature T_m . The specific heat jump at T_g is $H_m d(\Delta\varepsilon_{lg}) / dT$ equal to $1.5 S_m$ in a wide fraction of glasses [40].

The existence of Phase 3 was discovered for the first time in the supercooled water [41,42] and extended to glacial phases [2,31]. It appeared later that Phase 3 was built by heating the melt from its glassy state and was the congruent configuron phase expected since many years at the percolation threshold of broken bonds at T_g [33,43]. The name of Phase 3 was extended to all phases having a reduced enthalpy which results by cooling from a first-order transition giving rise to an exothermic enthalpy at their nucleation temperature. The first-order character disappears during the second cooling after subsequent heating above this new temperature T_g and leads to the zero enthalpy of glassy phase with an increased transition temperature T_g during the next heating.

Consequently, the formation of stable and ultrastable glasses by vapor deposition and glacial phases by heating or annealing glass-forming melts above T_g induces new liquid states having higher glass transition temperatures. This new point is generally not considered in the analysis of properties attached to polyamorphism. The new glass transition determines the new liquid phases at higher temperatures.

High heating rate increases the glass transition temperature [44]. Recent studies showed two associated transitions to glacial phases for various heating rates [35]. Exothermic transitions were observed during the first heating at the nucleation temperature of glacial phases followed, at higher temperatures, by endothermic glass transitions. Such observations are also found in molecular dynamics simulation of silver and silver alloys [45,46]. These findings confirmed that the glass transition characterizes Liquids 1 and 2 and Phase 3 and any change of T_g induces new liquid state.

Second melting temperatures of pure elements were predicted in 2007 [36]. At this time, it was already known that crystals covered by a solid thin film or imbedded into a matrix could melt at higher temperatures than T_m by homogeneous nucleation in crystal hearts instead of surface melting [47–50]. This idea was relaunched in glass-forming melts accompanied by predictions of their melting temperatures $T_{n+} > T_m$ using the non-classical model of homogeneous nucleation [1,33,34,51] confirmed by experimental observations [52–68]. These predictions had established that the medium-range order persists in liquids from T_g up to T_{n+} due to residual bonds producing endothermic enthalpy or due to antibonds producing exothermic enthalpy at T_{n+} where the homogeneous state of liquids appears. There are several temperatures T_{n+} in non-congruent materials associated with the various solidus and liquidus temperatures [1]. Exothermic enthalpy is always obtained after heating quenched melt far from below T_g or after heating stable and ultrastable glass and during formation of Phase 3 above T_g [33,34]. Residual and new bonds are also associated with slow heating and cooling of the melt. Annealing a melt between T_m and T_{n+} induces bonds and may develop bond percolation leading to crystallization at T_m without undercooling. The temperatures T_{n+} are not easy to recognize because they are mixed with liquidus temperatures in non-congruent materials [69–71].

The glassy state in liquid elements was determined with ε_{ls0} and $\varepsilon_{gs0} = 0.217$ corresponding to the mean value 0.103 of their Lindemann coefficient. The enthalpy coefficients $\Delta\varepsilon_{lg0}$ of Phase 3 being equal to zero at T_m , the glass transition occurs at T_g during cooling through a first-order transition and an exothermic latent heat equal to $\Delta\varepsilon_{lg}(\theta_g)$ [72].

Liquid ^4He in a confined space under pressure is amorphous and undergoes a transition during heating which looks like a first-order transition [73–75].

The aim of this work is to predict the melting temperatures of pure elements having a Lindemann coefficient around to 0.103 with the NCHM model [72,76]. New values of Lindemann constants for each element [77] are used to calculate the glass transition temperature of elements at low and high heating and cooling rates, the transition temperatures of glacial phases and the various melting temperatures of Ag, Cu, Zr, Ta, Re, Ni and Co compared with those deduced from MD simulations or from crystallization enthalpy of highly supercooled liquid elements.

2. Thermodynamic Consequences of Bonds or Antibonds Presence above T_m

The enthalpy recovery during heating up to T_{n+} is endothermic for bonds and exothermic for antibonds breaking [1]. The new melting entropy S depends on the reduced temperature θ_{n+} because this homogeneous nucleation temperature occurs for the enthalpy change $\Delta\varepsilon_{1g}(\theta_{n+})$ [1] and S is given in Equation (3):

$$S = \frac{H_m}{T_m} \pm \frac{\theta_{n+} H_m}{T_{n+}} = \frac{H_m}{T_m} \left(1 \pm \frac{\theta_{n+}}{1 + \theta_{n+}} \right) \quad (3)$$

The melting entropy S with antibonds is weaker than $S_m = H_m/T_m$ and equal to H_m/T_{n+} instead of H_m/T_m while total melting heat at T_{n+} is still equal to H_m . Two separate melting temperatures with antibonds exist: the first one at T_m producing an entropy equal to S_m and the second one at T_{n+} reducing the total entropy S . Consequently, a full melting temperature T_{n+} can exist without changing the total melting heat H_m . This metastable phase could be a glass up to T_{n+} if the glass escapes from crystallization with high heating rates. This temperature is observed with high heating rates after the formation of glass and glacial phases at lower temperatures. A residual exothermic latent heat is still observed in some glass-forming melts with heating rates R^+ equal to 0.33–0.66 K/s [53,54,62,63] while $R^+ \cong 10^{12}$ – 10^{13} K/s in liquid elements leads to full melting at T_{n+} [45,78,79]. The crystallization entropy is expected to be equal to $S_m / (1 + \theta_{n+})$ and the crystallization enthalpy $H_m / (1 + \theta_{n+})$ after the formation of glacial phases inducing early crystallization at lower cooling rates. Crystallization occurs by heating and formation of a fraction of bonds equal to a new critical threshold after quenching from homogeneous liquid state above T_{n+} . The melting entropy is increased when a percolation threshold of bonds is achieved at T_{n+} . This increase is due to the nucleation of a bond percolation threshold by still-lower heating rates following low cooling rates below T_g from above T_{n+} . The melting is produced when the configurational percolation occurs. The crystallization occurs at T_m after slow cooling from homogeneous melts when the bond number becomes equal to the percolation threshold [34,35,65,66]. It is important to note that the crystallization entropy loss below T_m is expected to be equal and opposite to the melting entropy observed above T_m at the temperature T_{n+} [1].

Weakened enthalpies and entropies are also observable for crystallization of highly undercooled glass-forming melts which are initially induced by glacial phase formation below T_m . The cases of tantalum and rhenium droplets, crystallized during free fall are examined as a first example [80]. High magnetic fields now replace free fall towers to study nucleation phenomena. A double transition leading to cobalt crystallization via glacial phase formation revealed a reduction of crystallization enthalpy under $B = 12$ Tesla and $B = 0$ [81].

3. Application of NCHN Model to Liquid Elements: First-Order Glass Transition during the First Cooling and Second-Order Transition during Heating

Enthalpy coefficients of liquid states 1, 2 and 3 are given in Equations (4)–(6) with $\theta_{0g}^2 = 1$, $\theta_{0m}^2 = 4/9$ and $\varepsilon_{1s0} = \varepsilon_{gs0}$ for pure liquid elements using Equations (1) and (2) [72]:

Liquid 1

$$\varepsilon_{1s} = \varepsilon_{1s0} \left(1 - \theta^2/4 \right) \quad (4)$$

Liquid 2

$$\epsilon_{gs} = \epsilon_{gs0} (1 - \theta^2) \tag{5}$$

Phase 3

$$\Delta\epsilon_{lg} = \epsilon_{ls} - \epsilon_{gs} = -1.25 \times \epsilon_{gs0} \times \theta^2. \tag{6}$$

New Lindemann coefficients δ_{ls} have been determined for many elements represented Figure 1 reprinted from [77]. The enthalpy coefficients $\epsilon_{ls0} = \epsilon_{gs0}$ of each element depending on δ_{ls} are given in Equation (7) [72]:

$$\delta_{ls} = (1 + \epsilon_{gs0})^{0.5} - 1 \tag{7}$$

1	2	3	4	5	6	7	8	9	10	11	12	13	14	15	16	17	18
η_1 0.139	η_2 0.113	-	η_4 0.119	η_5 0.136	η_6 0.109	η_7 0.12	η_8 0.084	η_9 0.07	η_{10} 0.111	η_{11} 0.108	η_{12} 0.08	-	-	η_{15} 0.095	-	-	-
1 H																	2 He
3 Li	4 Be											5 B	6 C	7 N	8 O	9 F	10 Ne
11 Na	12 Mg											13 Al	14 Si	15 P	16 S	17 Cl	18 Ar
19 K	20 Ca	21 Sc	22 Ti	23 V	24 Cr	25 Mn	26 Fe	27 Co	28 Ni	29 Cu	30 Zn	31 Ga	32 Ge	33 As	34 Se	35 Br	36 Kr
37 Rb	38 Sr	39 Y	40 Zr	41 Nb	42 Mo	43 Tc	44 Ru	45 Rh	46 Pd	47 Ag	48 Cd	49 In	50 Sn	51 Sb	52 Te	53 I	54 Xe
55 Cs	56 Ba	57 *La	58 Hf	59 Ta	60 W	61 Re	62 Os	63 Ir	64 Pt	65 Au	66 Hg	67 Tl	68 Pb	69 Bi	70 Po	71 At	72 Rn
87 Fr	88 Ra	89 †Ac	104 Rf	105 Db	106 Sg	107 Bh	108 Hs	109 Mt	110 Ds	111 Rg	112 Cn	113 Nh	114 Fl	115 Mc	116 Lv	117 Ts	118 Og

Figure 1. Lindemann coefficients of liquid elements distributed along columns of periodic table of elements by Mendeleev. The Lindemann coefficients δ_{ls} along Line 2 for each column. Reprinted with permission from [77]. Copyright 2019 Elsevier.

The reduced glass transition temperature θ_g occurs at the homogeneous nucleation temperature $\theta_{n-} = [\epsilon_{gs} (\theta_{n-}) - 2] / 3$ [1] which is given in Equation (8) equivalent to Equation (2) with $\Delta\epsilon = 0$, $\theta_{n-} = \theta_g$ and $\theta_{0g}^2 = 1$:

$$\epsilon_{gs0} = (3 \times \theta_{n-} + 2 - \Delta\epsilon) / (1 - \theta_{n-}^2) \tag{8}$$

The glass transition reduced temperatures are represented in Figure 2 for all Lindemann coefficients of Figure 1 together with the reduced transformation temperature θ_D above which the liquid is homogeneous in the absence of glacial phase melting above T_D . This temperature T_D occurs at the homogeneous nucleation temperature above T_m given in Equation (9) for $\theta_{0m}^2 = 4/9$ applied using Liquid 1 which has a lower enthalpy coefficient ϵ_{ls} than that of Liquid 2 above T_m :

$$\theta_D = \epsilon_{ls}(\theta_D) = \epsilon_{ls0} (1 - \theta_D^2 \times \theta_{0m}^{-2}) \tag{9}$$

The new Lindemann coefficient δ_{ls} of Ag and Cu is 0.108 instead of 0.103 used in a previous publication [76]. The new Ag enthalpy coefficients of Liquids 1, 2, and 3 are represented in Figure 3 with $\epsilon_{ls0} = \epsilon_{gs0} = 0.22766$ determined with Equation (7). Line 1 is attached to Liquid 1, 2 to Liquid 2 and 3 and 4 to Phase 3.

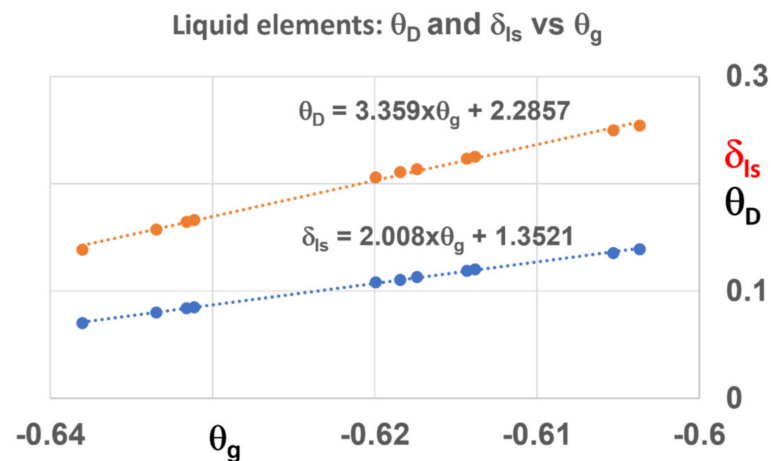


Figure 2. The Lindemann coefficient δ_{1s} and the reduced homogeneous nucleation temperature $\theta_D = (T_D - T_m)/T_m$ of liquid elements in the absence of overheated Phase 3 above T_D versus the reduced glass transition temperature $\theta_g = (T_g - T_m)/T_m$.

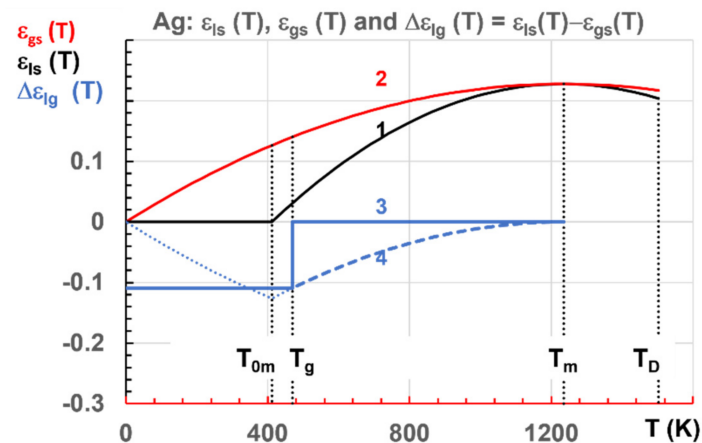


Figure 3. Ag enthalpy coefficients: liquids 1, 2 and 3–4 versus temperature in Kelvins. $T_g = 469.34$ K, $T_{0m} = T_m/3 = 411.63$ K, $T_D = 1489$ K, $\varepsilon_{1s0} = \varepsilon_{gs0} = 0.22766$, $\theta_{0m}^2 = 0.444445$ and $\theta_{0g}^2 = 1$ in Equations (4)–(6).

During the first cooling from homogeneous liquid state [1], Phase 3 follows Line 3 ($\Delta\varepsilon_{1g} = 0$) down to the homogeneous nucleation temperature $T_g = 469.34$ K where a first-order transition with an exothermic latent heat $\Delta\varepsilon_{1g} \times H_m = -0.10937H_m$ occurs, giving rise to a constant enthalpy below T_g [2] (pp. 42,43). The first heating from the glassy state follows line 4 because the formation of configurons leads to a second-order phase transition. Phase 3 in liquid elements would disappear at T_m in the absence of glacial phase. Recent MD simulations show the first-order character of all glacial phase transitions occurring during the first cooling which is confirmed with the NCHN model [45,76]. The various enthalpy reductions are cumulated during the cooling rate and are maintained during heating up to the glass transition temperature of phases. These various events are predicted using the homogeneous nucleation temperatures associated with liquids 1, 2 and 3. The latent heat of glass-phase formation is progressively recovered by heating between T_g and T_m .

The main conclusions of this chapter are the first-order character of the transition from liquids state to the glassy state and the second-order phase transition from the glassy state to the ordered Liquid 3 along Line 4 in Figure 3. This point was not raised in previous publications considering that the first-order character was reversible [72,75,76].

4. Singular Values of Enthalpy of Glacial Phases in Liquid Elements

Glacial phases enthalpy in glass-forming melts have singular values after the first cooling: 0 for the current glass state, $-H_m \Delta\epsilon_{lg0} = -H_m (\epsilon_{ls0} - \epsilon_{gs0})$, $-H_m \Delta\epsilon_{lg0}/2$, $H_m \Delta\epsilon_{lg}(\theta_{0m})$, and $-H_m$ giving rise to crystals. The nil value could correspond to equal numbers of bonds and antibonds at the percolation threshold of bonds at T_g . The values $-\Delta\epsilon_{lg0}$ and $-\Delta\epsilon_{lg0}/2$ were involved in the formation of stable and ultrastable glasses and gave rise to zero enthalpy and an increase of T_g during the second cooling [1,2,33,34]. The value $\Delta\epsilon_{lg}(\theta_{0m})$ defined the glacial phase enthalpy of $Mg_{69}Zn_{27}Yb_4$ leading to quasi-crystalline phase of same enthalpy [32,33]. These singular values could correspond to higher percolation thresholds leading to higher T_g and to the glassy phases or metastable crystalline phases already analyzed for various ice amorphous phases [82,83].

Singular enthalpies of glacial phases also exist in liquid elements as already shown [76]. The nil enthalpy has disappeared except in the homogeneous liquid state above T_{n+} . This homogeneous liquid state can be prolonged by rapid cooling down to T_m . Phase 3 has a negative enthalpy equal to the latent heat of vitrification of various elements at T_g . The other enthalpy coefficients are $-\epsilon_{ls0} = -\epsilon_{gs0}$, the minimum value $-1.25 \epsilon_{ls0}$ at 0 K, and $\Delta\epsilon_{lg}(\theta_{0m})$. Figure 4 shows these values for Ag. Table 1 gives the singular values of enthalpy coefficients for each element given in Figure 1.

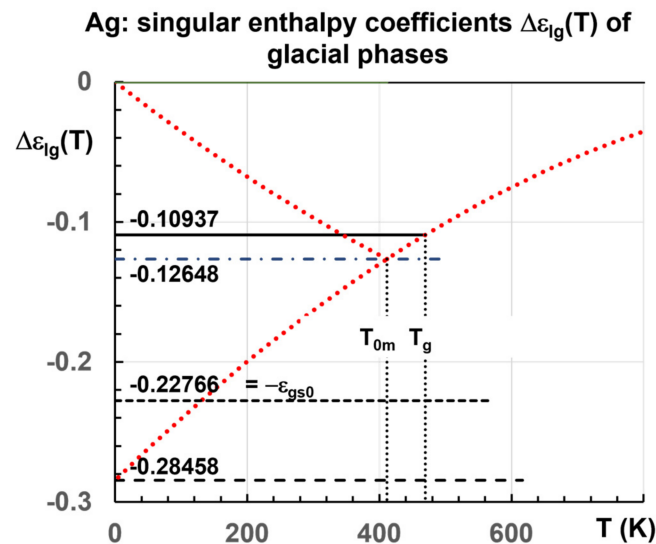


Figure 4. Enthalpy coefficients of Ag Phase 3 versus Temperature in Kelvins with singular values.

Table 1. Lindemann coefficients δ_{ls} , singular values of enthalpy coefficients $-\epsilon_{ls0} = -\epsilon_{gs0}$, $\Delta\epsilon_{lg}(\theta_{0m})$, $-1.25\epsilon_{ls0}$, $\Delta\epsilon_{lg}(\theta_g)$, being fractions of melting enthalpy of liquid elements. All elements, in the same column of Figure 1, have identical singular enthalpy coefficients. T_m , T_g and T_D are in Kelvin.

	δ_{ls}	ϵ_{gs0}	$\Delta\epsilon_{lg}(\theta_{0m})$	$1.25 \epsilon_{gs0}$	$\Delta\epsilon_{lg}(\theta_g)$	θ_g	T_m	T_g	T_D
Li	0.139	-0.29732	-0.16518	-0.37165	-0.13544	-0.60368	464	184	581
Ta	0.136	-0.29050	-0.16139	-0.36312	-0.13305	-0.60531	3288	1298	4109
Re	0.12	-0.25440	-0.14133	-0.31800	-0.11981	-0.61382	3458	1335	4237
Zr	0.119	-0.25216	-0.14009	-0.31520	-0.11896	-0.61433	2125	820	2600
Mg	0.113	-0.23877	-0.13265	-0.29846	-0.11377	-0.61741	923	353	1121
Ni	0.111	-0.23432	-0.13018	-0.29290	-0.11202	-0.61843	1728	659	2092
Ag	0.108	-0.22766	-0.12648	-0.28458	-0.10937	-0.61994	1235	469	1489
As	0.095	-0.19903	-0.11057	-0.24878	-0.08824	-0.62635	1090	407	1290
Fe	0.084	-0.17506	-0.09725	-0.21882	-0.08729	-0.63159	1811	667	2109
Zn	0.08	-0.16640	-0.09244	-0.20800	-0.08346	-0.63345	693	254	801
Co	0.07	-0.14490	-0.08050	-0.18113	-0.07368	-0.63780	1768	640	2013

5. Universal Law for the Second Melting Temperature T_{n+} Depending on the Homogeneous Nucleation Temperature T_{nG} of Glacial Phases

The glass transition temperature T_g increases with the Lindemann coefficient in Figure 2. Increasing the heating rate rises the T_g . The NCHM model uses an increased Lindemann coefficient to predict T_g and T_{nG} at higher heating rates. Consequently, to each value of θ_g corresponds a value of $\varepsilon_{ls0} = \varepsilon_{gs0}$ given by Equation (8) with $\Delta\varepsilon = 0$ and new laws for $\varepsilon_{ls}(\theta)$, $\varepsilon_{gs}(\theta)$ and $\Delta\varepsilon_{lg}(\theta)$ are established preserving $\theta_{0g}^2 = 1$ and $\theta_{0m}^2 = 4/9$. At the homogeneous nucleation reduced temperature θ_{nG} of glacial phase, a difference of enthalpy $\Delta\varepsilon_{lg}(\theta_{nG}) = -\theta_{n+}$ must be induced to obtain its melting at θ_{n+} [1]. The values of $\varepsilon_{gs0} = \varepsilon_{ls0}$ are higher than 2 in Table 2 because the melting temperature T_m is used instead of T_{n+} to predict T_{n+} . Using the new melting temperature T_{n+} , these coefficients would not be higher than 2.

Table 2. Examples of second melting temperatures T_{n+} and nucleation temperatures T_{nG} of glacial phases of Tantalum, Rhenium, Zirconium, Silver, Iron, Copper and Cobalt above T_m . For $\theta_g = \theta_{n+}$ equal to singular values of enthalpy coefficients; ε_{gs0} deduced from Equation (8) with $\Delta\varepsilon = 0$; θ_{nG} the reduced nucleation temperature of glacial phase leading to $\Delta\varepsilon_{lg}(\theta_{nG}) = \varepsilon_{ls}(\theta_{nG}) - \varepsilon_{gs}(\theta_{nG}) = -\theta_{n+}$; $\varepsilon_{ls}(\theta_{nG})$ and $\varepsilon_{gs}(\theta_{nG})$ deduced from Equations (4) and (5); temperatures T_{n+} in Kelvin; ratios T_{n+}/T_m and T_{nG}/T_m .

	$\theta_g = \theta_{n+}$	ε_{gs0}	θ_{nG}	T_{nG}	$\varepsilon_{ls}(\theta_{nG})$	$\varepsilon_{gs}(\theta_{nG})$	$\Delta\varepsilon_{lg}(\theta_{nG})$	$\theta_{n+}(\theta_{nG})$	T_{n+}	T_{n+}/T_m	T_{nG}/T_m
Ta	0.29050	3.13616	0.27222	4183	2.61326	2.90376	-0.29050	0.29050	4243	1.29050	1.27222
Re	0.31800	3.28633	0.27823	4420	2.71392	3.03193	-0.31800	0.31800	4558	1.318	1.27823
Zr	0.11896	2.39071	-0.19952	1701	2.17658	2.29554	-0.11896	0.11896	2378	1.11896	0.80048
Ag	0.12648	2.41812	-0.20456	982	2.19045	2.31694	-0.12648	0.12648	1391	1.12648	0.79544
Fe	0.21882	2.79005	-0.25049	1357	2.39618	2.61500	-0.21882	0.21882	2207	1.21866	0.74951
Cu	0.35413	3.50151	0.28445	1744	2.86407	3.21820	-0.35413	0.35413	1839	1.35413	1.28445
Co	0.0805	2.25612	-0.16895	1469	2.11122	2.19172	-0.0805	0.0805	1910	1.0805	0.83105
Max	0.47	4.37685	0.29310	-	3.53084	4.00084	-0.47001	0.47001	-	1.47000	1.29310

Equations (4)–(8) are applied at a second melting temperature with $\theta_g = \theta_{n+}$ for several elements as shown in Table 2. The θ_{n+} values are experimental values applying high heating rates in MD simulations [45,78,79] or observing early crystallization during droplet free fall [80] or under high magnetic field [81]. The reduced temperature $\theta_g = \theta_{n+}$ is the highest glass transition temperature in a liquid having a reduced melting temperature equal to θ_{n+} . The reduced melting temperatures θ_{n+} are chosen equal to singular values of enthalpy coefficients of various elements in agreement with those of Table 1 respecting the nucleation law $\Delta\varepsilon_{lg} = \theta_{n+} = \theta_g$ [1,36]. This calculation is extended to higher values of $\theta_g = \theta_{n+}$ up to 1. The highest melting temperature for the highest heating rate is $2 T_m$ with a total entropy $S_m/2$. For this the enthalpy $\Delta\varepsilon_{lg}$ is equal to zero and the number of antibonds would be equal to that of bonds. The total enthalpy for two separated melting temperatures at T_m and $2 T_m$ would be $H_m/2$.

There is a maximum nucleation temperature of glacial phase equal to $1.2931 T_m$ even if the existence of much higher glass transition temperatures $\theta_g = \theta_{n+}$ above $1.47 T_m$ is possible as shown in Figure 5. The value of θ_{n+} for Cu is much higher than that given for Ag in Table 1. The coefficient 0.35413 is the sum of 0.22766 and 0.12648. This enhancement is expected for a double transition above T_m . It is difficult to envisage a full melting temperature far above $\theta_{n+} = 0.47$ because triple transitions above T_m would be involved. The transition at $\theta_{n+} = 1$ (not represented in Figure 5) exists because $\Delta\varepsilon_{lg}$ could be equal to the singular value $\Delta\varepsilon_{lg} = -1$.

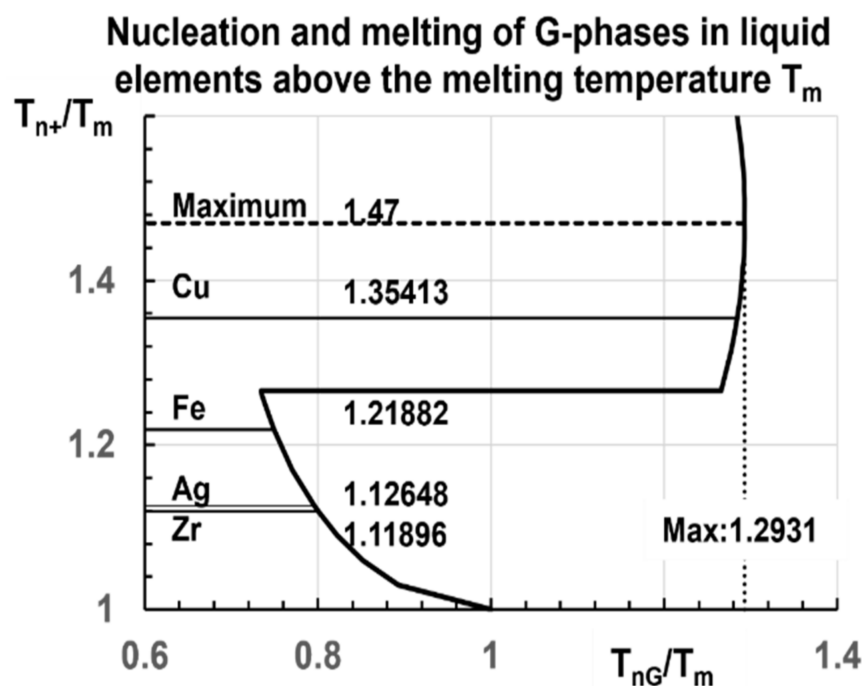


Figure 5. Universal diagram of T_{n+}/T_m versus T_{nG}/T_m of all liquid elements with higher and higher heating rates. The ratios $T_{n+}/T_m = 1.11896$ for Zr ($T_{n+} = 2378$ K, $T_m = 2125$ K) [79], 1.12648 for Ag ($T_{n+} = 1391$ K, $T_m = 1234.9$ K) [45], 1.21882 for Fe ($T_{n+} = 2207$ K, $T_m = 1811$ K) [78], and 1.35413 for Cu ($T_{n+} = 1839$ K, $T_m = 1358$ K) [78] had been already observed by MD simulations at various high heating rates as shown in Figures 5–7.

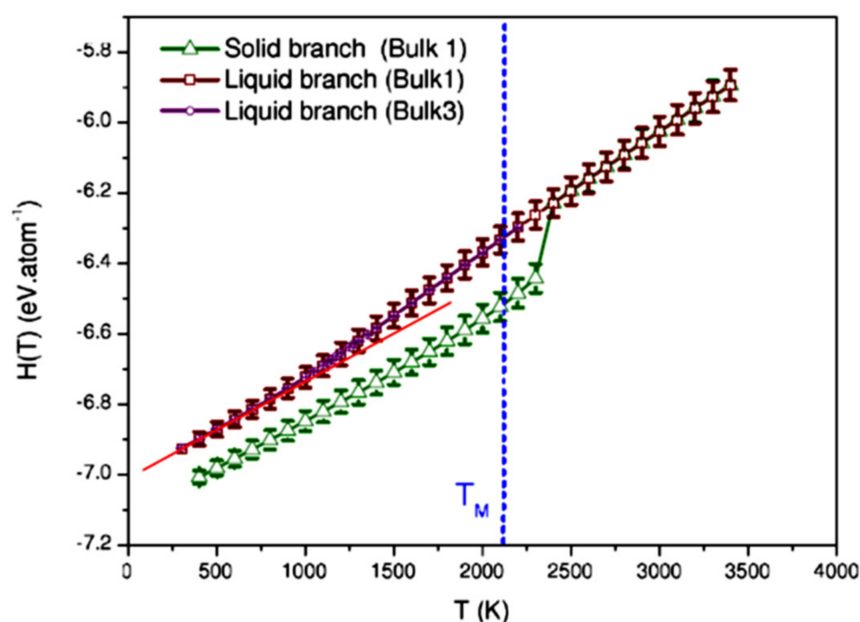


Figure 6. MD simulations of liquid zirconium enthalpy observing a melting temperature of 2378 K instead of $T_m = 2125$ K. Reprinted with permission from [79]. Copyright American Physical Society 2020.

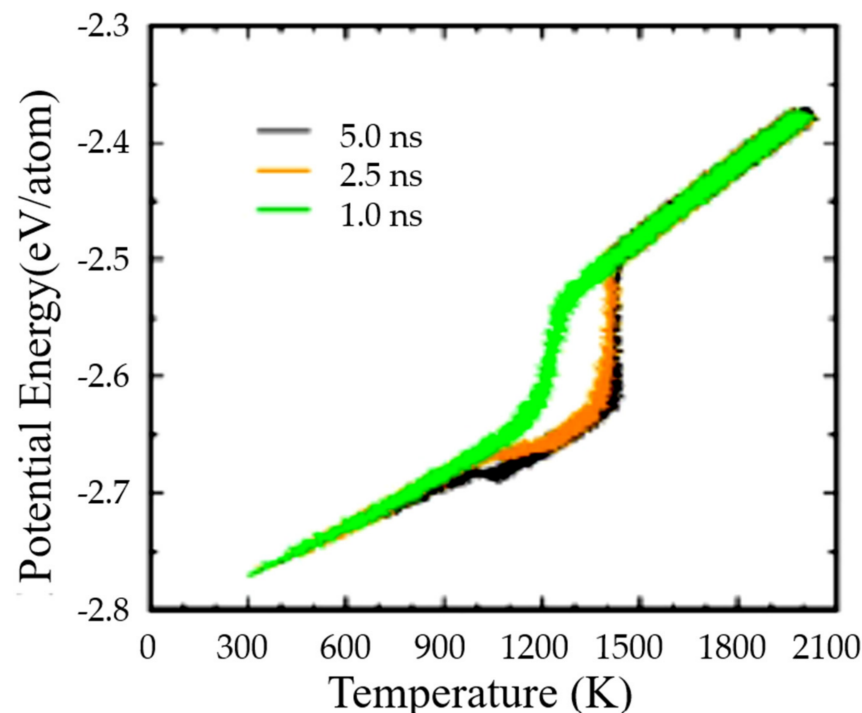


Figure 7. MD simulations of liquid silver observing a melting temperature of 1391 K during heating a 32,000 atoms system instead of $T_m = 1234.9$ K (5 ns with $R = 0.34 \times 10^{12}$ K/s, 2.5 ns with $R = 0.68 \times 10^{12}$ K/s and 1 ns with $R = 1.7 \times 10^{12}$ K/s). Reprinted with permission from [45]. Copyright 2020 American Chemistry Society ACS.

6. Observations of Second Melting Temperatures T_{n+} with MD Simulations

6.1. Zirconium

The nucleation temperature of Zr glassy phase occurred at $T_g = 1000$ K during the first cooling as shown in Figure 6 by [79] and predicted in Chapter 7. A second melting temperature at $T_{n+} = 2378$ K instead of $T_m = 2125$ K was obtained during heating after quenching the liquid below T_g and applying a mean heating rate $R = +10^{12}$ K/s. The glass transition temperature T_g of glacial phase was equal to T_{n+} as shown in Figure 6.

6.2. Silver

Figure 7 published by [45] represented a sharp transition during heating at $T_{n+} = 1391$ K of liquid silver, corresponding to a liquid-glass transition at T_{n+} . The nucleation temperature of glacial phase occurred at $T_{nG} = 957$ K during the heating as predicted in Chapter 7. The glass transition of Liquids 1 and 2 was $T_m = 1234.9$ K while that of glacial phase was equal to T_{n+} corresponding to θ_{n+} (θ_{nG}) = 0.12468. A very high enthalpy change resulting from the first-order transitions during previous cooling was observed before undergoing the nucleation temperature T_{nG} of the glacial phase.

In Figure 8, the transition at $T_{nG} = 917$ K with $\epsilon_{ls0} = \epsilon_{gs0} = 1.53040$ induces a liquid phase having an enthalpy coefficient equal to -1 instead of -0.12648 and a melting temperature $T_{n+} = 1391$ K. The enthalpy coefficient varies from -1 to zero at $T_{n+} = 1391$ K.

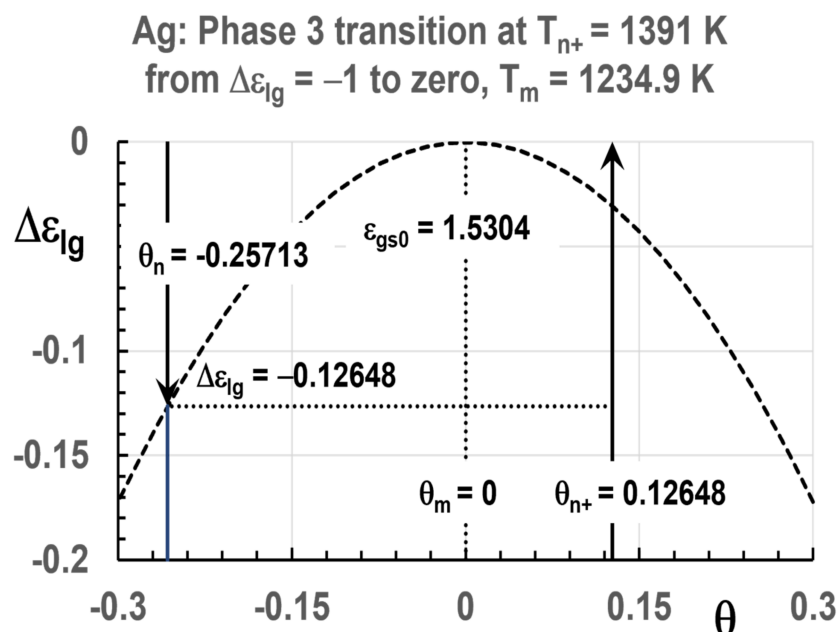


Figure 8. Ag Phase 3 enthalpy coefficient $\Delta\varepsilon_{lg}(\theta) = \varepsilon_{ls} - \varepsilon_{gs}$ with $\varepsilon_{ls0} = \varepsilon_{gs0} = 1.53040$ plotted versus θ . $\theta_{nG} = -0.25713$, $\Delta\varepsilon_{lg}(\theta_{nG}) = -0.12648$ inducing $\Delta\varepsilon_{lg} = -1$ due to the proximity of T_m . Melting at $T_{n+} = 1391$ K.

6.3. Iron and Copper

The glassy phases occurred at 800 K for Cu and 1100 K for Fe as reproduced in Figure 9 and predicted in Chapter 7 [78]. Second melting temperatures $T_{n+} = 1839$ K instead of $T_m = 1358$ K for Cu and $T_{n+} = 2207$ K instead of $T_m = 1811$ K for Fe were observed, applying heating and cooling rates $R = \pm 10^{13}$ K/s. The glass transition temperatures T_g of glacial phases were equal to T_{n+} .

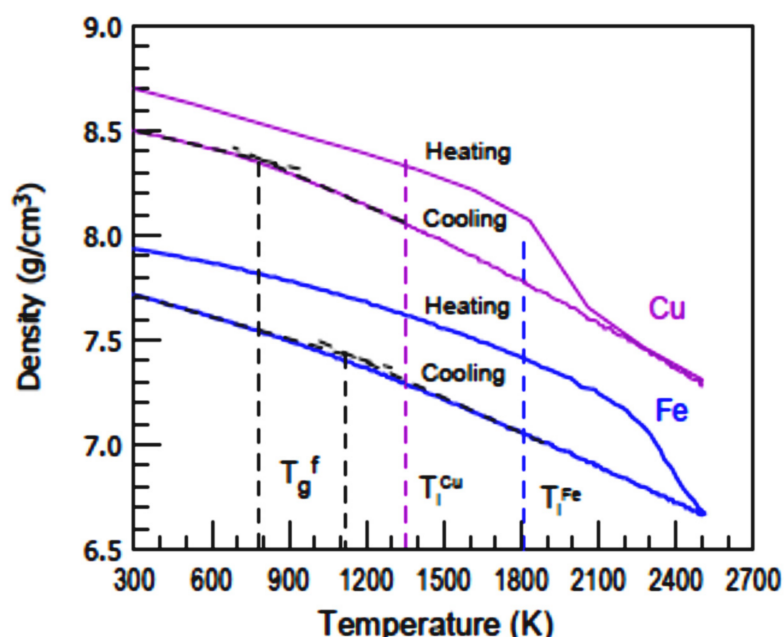


Figure 9. MD simulations of liquid copper density observing a melting temperature of 1839 K instead of $T_m = 1358$ K and MD simulations of liquid iron density observing a melting temperature of 2207 K instead of $T_m = 1811$ K. $R = \pm 10^{13}$ K/s. Reprinted with permission from Ref. [78].

7. Glacial Phases Formation below T_m with Singular Enthalpies with MD Simulations

7.1. Silver

The steady-state relaxation time is given by Equation (10)

$$\ln(\tau_1/s) = B_1/(T - T_m/3) + \ln(\tau_0/s) \quad (10)$$

with $B_1 = 1171.35$ K, $T_m/3 = 411.63$ K and $\ln(\tau_0 (s)) = -25.714$ and where it was used to predict in Table 3 the glacial phase transition temperatures θ_{nG} of liquid silver during various heating and cooling rates referring to a system of 256,000 atoms reproduced in Figure 10 for few cooling rates R [45]. The value $\ln(R)$ is used to determine $T = T_g$ with Equation (10).

Table 3. Nucleation temperatures T_{nG} of Ag glacial phases below T_m . T_g and θ_g for various values of heating and cooling rates R in K/s; ϵ_{gs0} deduced from Equation (8) with $\Delta\epsilon = 0$; θ_{nG} the reduced nucleation temperature of glacial phase leading to singular values $\Delta\epsilon_{lg}(\theta_{nG}) = \epsilon_{ls}(\theta_{nG}) - \epsilon_{gs}(\theta_{nG}) = -\theta_{n+}$; $\epsilon_{ls}(\theta_{nG})$ and $\epsilon_{gs}(\theta_{nG})$ deduced from Equations (4) and (5); temperatures T_{nG} ; R (K/S) and $\ln R$ introduced in Equation (10) to determine T_g (K).

1	2	3	4	5	6	7	8	9	10	11
2	T_g (K)	θ_g	ϵ_{gs0}	θ_{nG}	$\epsilon_{ls}(\theta_{nG})$	$\epsilon_{gs}(\theta_{nG})$	$\Delta\epsilon_{lg}(\theta_{nG})$	T_{nG} (K)	R (K/s)	$\ln R$
					Heating					
3	1200	-0.02826	0.88766	-0.33762	0.66000	0.78648	-0.12648	818	2.27×10^{12}	28.45
4	1110.6	-0.10066	1.71541	-0.32584	1.30562	1.53328	-0.22766	832.5	1.7×10^{12}	28.162
5	1023	-0.17154	1.53040	-0.25713	1.30274	1.42922	-0.12648	917	1.18×10^{12}	27.797
					Cooling					
6	925	-0.25095	1.33097	-0.41358	0.81873	1.10331	-0.28457	724	-6.80×10^{11}	27.245
7	839	-0.32059	1.15715	-0.39673	0.74736	0.97502	-0.22766	745	-3.40×10^{11}	26.55
8	785.6	-0.36384	1.04711	-0.34755	0.76252	0.92063	-0.15810	806	-1.88×10^{11}	25.959
9	686.4	-0.44417	0.83156	-0.32438	0.63468	0.74406	-0.10937	834	-3.40×10^{10}	24.249

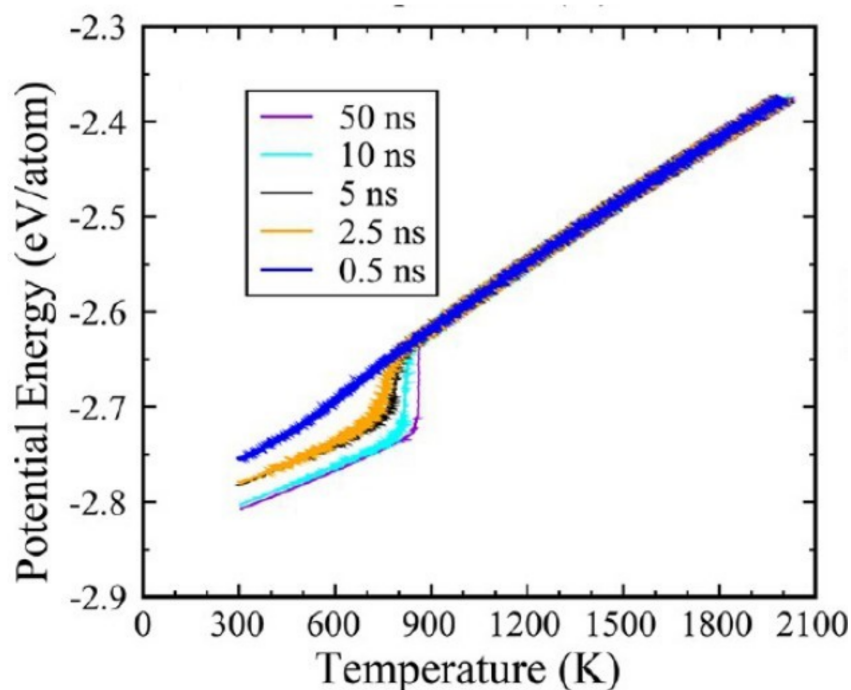


Figure 10. Cooling of a 256,000 atoms system with various cooling rates. -3.4×10^{12} (0.5 ns), -6.8×10^{12} (2.5 ns), -3.4×10^{12} (5 ns), -1.7×10^{11} (10 ns), and -0.34×10^{11} (50 ns) K/s. These transformation temperatures are predicted in Table 3-cooling. Reprinted with permission from [45]. Copyright 2020 American Chem. Society ACS.

The NCHN model shows that weaker cooling rates induce higher nucleation temperatures of glacial phases with singular enthalpy values in agreement with MD simulations of

An Q. et al. in Figure 10. A new singular value -0.15810 is added in Table 3 (Line 8) for the transition at $T_{nG} = 806$ K. It is equal to the difference between the singular values -0.28458 and -0.12648 given in Table 1, corresponding to the reduction of the enthalpy coefficient of Phase 3 from $\theta = \theta_{0m}$ to its minimum value at $\theta = -1$ in Figure 4. Other singular values are expected with $T_g = T_m$ in Table 4 (Lines 14–16), -0.10937 ($T_{n+} = 1370$ K), -0.12648 ($T_{n+} = 1391$ K) and -0.15810 ($T_{n+} = 1460$ K), varying the heating rate. The temperatures T_{nG} are equal to 977 K (Line 14), and 957 K (Line 15) in agreement with MD simulations in Figure 7 [45]. The coefficient -0.15810 (Line 16) would lead to $T_{nG} = 852$ K.

Table 4. Application of NCHN model to Ta, Zr, Ni, Ag, Cu, Fe and Co. θ_g and T_g for various heating and cooling rates R in K/s; ϵ_{gs0} deduced from Equation (8) with $\Delta\epsilon = 0$; θ_{nG} the reduced nucleation temperature of glacial phase leading to singular values $\Delta\epsilon_{lg}(\theta_{nG}) = \epsilon_{ls}(\theta_{nG}) - \epsilon_{gs}(\theta_{nG}) = -\theta_{n+}$; $\epsilon_{ls}(\theta_{nG})$ and $\epsilon_{gs}(\theta_{nG})$ deduced from Equations (4) and (5); temperatures T_{nG} ; $T_{n+} = (1 + \Delta\epsilon_{lg}(\theta_{nG})) \times T_m$.

	δ_{ls}	θ_g	T_g	ϵ_{gs0}	θ_{nG}	T_{nG}	$\epsilon_{ls}(\theta_{nG})$	$\epsilon_{gs}(\theta_{nG})$	$\Delta\epsilon_{lg}(\theta_{nG})$	θ_{n+}	T_{n+}	T_m	Ref.
Ta													
1	0.136	0.00000	3288	2.00000	-0.23070	2529	1.76050	1.89356	-0.13306	0.13305	3725	3288	
2	0.136	0.00000	3288	2.00000	-0.25408	2453	1.70950	1.87089	-0.16139	0.16139	3819	3288	
3	0.136	-0.49817	1650	0.67235	-0.39788	1980	0.43286	0.56591	-0.13305	0.13305	3725	3288	[84]
4	0.136	-0.49817	1650	0.67235	-0.4382	1847	0.38187	0.54325	-0.16139	0.16139	3819	3288	[84]
Zr													
5	0.119	0.00000	2125	2.00000	-0.21814	1661	1.78587	1.90483	-0.11896	0.11896	2378	2125	
6	0.119	0.00000	2125	2.00000	-0.23672	1622	1.74784	1.88793	-0.14009	0.14009	2423	2125	
7	0.119	-0.52941	1000	0.57212	-0.40785	1258	-0.35799	-0.47695	-0.11896	0.11896	2378	2125	[79]
8	0.119	-0.52941	1000	0.57212	-0.44259	1184	0.31996	0.46005	-0.14009	0.14009	2423	2125	[79]
9	0.119	-0.58118	890	0.38727	-0.49573	1072	0.17313	0.29209	-0.11896	0.11896	2378	2125	[79]
Ni													
10	0.111	0.00000	1728	2.00000	-0.21168	1362	1.79836	1.91038	-0.11202	0.11202	1922	1728	
11	0.111	0.00000	1728	2.00000	-0.22819	1334	1.76568	1.89586	-0.13018	0.13018	1953	1728	
12	0.111	-0.33449	1150	1.12207	-0.28261	1240	0.92043	1.03245	-0.11202	0.11202	1922	1728	[85]
13	0.111	-0.4618	930	0.7812	-0.3387	1143	0.57956	0.69158	-0.11202	0.11202	1922	1728	[86]
Ag													
14	0.108	0.00000	1234.9	2.00000	-0.20916	977	1.80313	1.91250	-0.10937	0.10937	1370	1234.9	[45]
15	0.108	0.00000	1234.9	2.00000	-0.22493	957	1.77233	1.89881	-0.12648	0.12648	1391	1234.9	[45]
16	0.108	0.00000	1234.9	2.00000	-0.30177	862	1.59021	1.81787	-0.22766	0.15810	1430	1234.9	
Cu													
17	0.108	0.00000	1358	2.00000	-0.30177	948	1.59021	1.81787	-0.22766	0.22766	1667	1358	[78]
18	0.108	-0.41090	800	0.92317	-0.33107	908	0.6955	0.82198	-0.12648	0.12648	1530	1358	[78]
Fe													
19	0.084	0.00000	1811	2.00000	-0.29585	1275	1.60613	1.82495	-0.21882	0.21882	2207	1811	[78]
20	0.084	-0.42736	1000	0.82123	-0.46169	975	0.42736	0.64618	-0.21882	0.21882	2207	1811	[78]
Co													
21	0.07	0	1768	2	-0.17948	1451	1.85504	1.93557	-0.0805	0.0805	1910	1768	[81]
22	0.07	-0.20136	1412	1.45491	-0.21039	1396	1.31001	1.39051	-0.0805	0.0805	1910	1769	[81]

7.2. Tantalum

A glass transition temperature T_g of 1650 K of tantalum was observed through ultrafast liquid quenching [84]. This value is used in Table 4 (Lines 4 and 5) to predict two possible values $T_{nG} = 1980$ K and 1847 K corresponding to the singular enthalpy coefficients -0.13305 and -0.16138 respectively. The same coefficients were obtained for $T_g = T_m$ (Lines 1 and 2).

7.3. Zirconium

Zr MD simulations during various quenching processes revealed two T_g values 1000 K and 890 K and a full melting at 2378 K [79]. The same singular coefficient -0.11896 leads to $T_{nG} = 1258$ and 1072 K as shown Lines 7 and 9 in Table 4 and full melting occurs at $T_{n+} = 2378$ K. For $T_g = 1000$ K (Line 8), T_{nG} can also be equal to 1184 K with an enthalpy coefficient of -0.14009 and $T_{n+} = 2423$ K. For $T_g = T_m$ (Lines 5 and 6), the two singular coefficients would be -0.11895 and -0.14009 with $T_{nG} = 1661$ and 1622 K leading to full melting at $T_{n+} = 2378$ and 2423 K, respectively.

7.4. Nickel

Ni MD simulations revealed two T_g values 1150 and 930 K [85,86]. They result from the same singular enthalpy coefficient -0.11202 , Lines 12 and 13 in Table 4, which would lead to $T_{nG} = 1240$ and 1143 K and to full melting at $T_{n+} = 1922$ K. A glass transition at $T_g = T_m$ would lead to $T_{n+} = 1922$ and 1953 K with singular enthalpy coefficients equal to -0.11202 and -0.13018 , respectively (Lines 10 and 11 in Table 4).

7.5. Copper

Cu MD simulations revealed a T_g value of 800 K in Figure 9 with a cooling rate of -10^{13} K/s [78]. It corresponds to $T_{nG} = 908$ K with a singular enthalpy coefficient $\Delta\epsilon_{lg}(\theta_{n+}) = -0.12648$ (Line 18 Table 4). For $T_g = T_m$ (Line 17 Table 4), $T_{nG} = 948$ K, $T_{n+} = 1667$ K.

7.6. Iron

Fe MD simulations revealed $T_g = 1000$ K in Figure 9 with a cooling rate of -10^{13} K/s [78]. It corresponds to $T_{nG} = 975$ K with a singular enthalpy coefficient $\Delta\epsilon_{lg}(\theta_{n+}) = -0.21882$ (Line 20 Table 4). For $T_g = T_m$ (Line 19 Table 4), $T_{nG} = 1275$ K, $\Delta\epsilon_{lg}(\theta_{n+}) = -0.21882$ and $T_{n+} = 2207$ K.

8. The Free Fall Solidification of Tantalum and Rhenium Droplets via Glacial Phases

The Ta and Re solidifications were observed in two steps during the free fall of overheated liquid droplets as shown in Figure 11 [80]. The undercooling (ΔT) down to 2770 K was 518 K with $T_m = 3288$ K and the crystallization occurred with two steps, the first one being the first-order transition of a glacial phase at 2770 K, inducing in the second step at 2930 K full crystallization and coalescence after an incubation time. For an adiabatic process, the coalescence led to the melting temperature T_m with a latent heat equal to $(\Delta T) \times C_p = 518 \times C_p$ [87], C_p being the average heat capacity of tantalum between 2770 and 3288 K given by Equation (11) [88]:

$$\Delta C_p = 25 + 5.87 \times 10^{-3} T \text{ in J/K/mole} \quad (11)$$

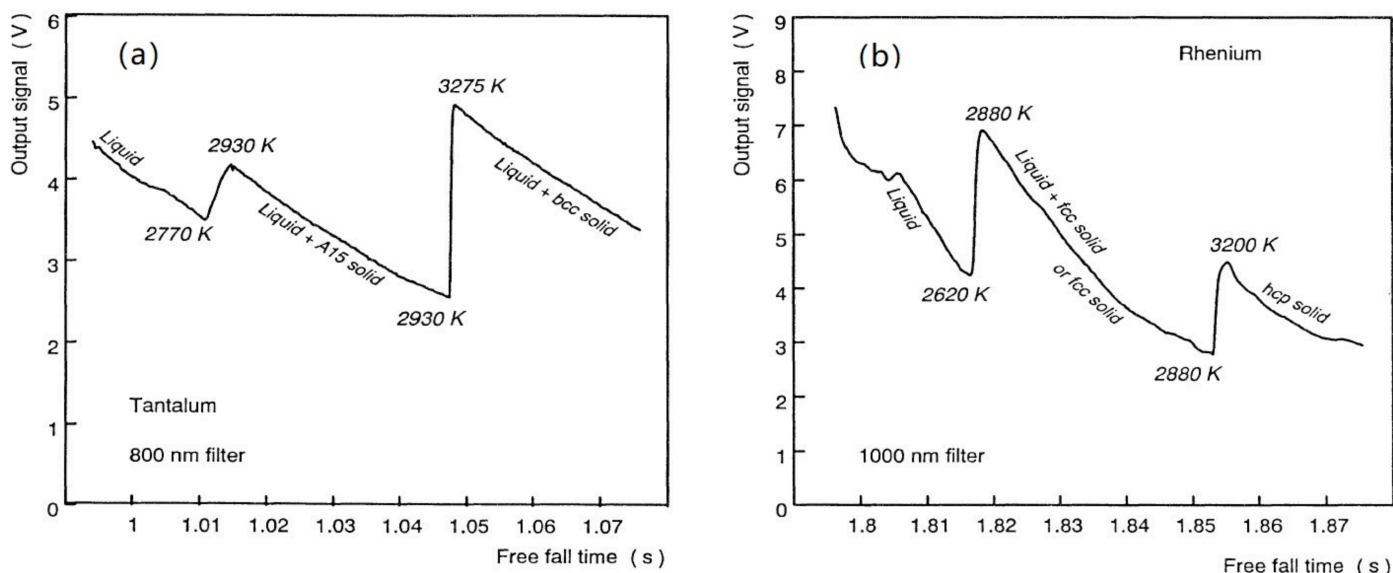


Figure 11. (a) Brightness trace during solidification of a tantalum droplet during its free fall. The two successive recalescence peaks show evidence of a double transformation phenomenon. (b): Brightness trace during solidification of a rhenium droplet during its free fall. The two successive recalescence peaks still show evidence of a double transformation phenomenon. Reprinted with permission from [80]. Copyright 1993 ACS.

Its average value for $2770 < T < 3288$ K was 42.83 J/K/mole and the solidification enthalpy 22186 J/mole representing 69.33% of the melting enthalpy 32 KJ/mole at T_m . The

experimental reduction was 0.3067 while the sum of two singular values $0.16139 + 0.10294 = 0.29444$ are predicted in Table 2. The agreement is good and $\theta_{n+}/(1 + \theta_{n+}) = 0.29444$ leads to $\theta_{n+} = 0.4424$.

The Re solidification was observed at 2620 K for $T_m = 3458$ K with undercooling $(\Delta T) = 838$ K. The heat capacity was given [89] by Equation (12):

$$\Delta C_p = 25 + 3.329 \times 10^{-3} T \text{ in J/K/mole} \quad (12)$$

The average heat capacity being 35.117 J/K/mole between 2620 and 3458 K, the solidification enthalpy was 29428 J/mole instead of 33230 Joules/mole for the melting enthalpy at T_m . The reduction was 11.44% corresponding to the singular coefficient of 0.11981 in Table 1. The temperature T_{n+} would be equal to $1.1361 T_m = 3929$ K. The heat capacity depends on the sample purity because a weaker value $2.29 \times 10^{-3} T$ had been measured at low temperatures [88]. Its average value for $2620 < T < 3458$ K was 31.96 J/K/mole. The enthalpy change was $31.96 \times 838 = 26782$ J/mole instead of 33230 J/mole corresponding to a total reduction of 19.4%. This reduction coefficient is too far from the singular coefficients of rhenium in Table 1.

9. The Two Peaks of Recalescence of Undercooled Cobalt in High Magnetic Field $B = 12$ Tesla and $B = 0$

The undercooling (ΔT) of liquid cobalt was increased after 20 cycles of temperature between 1873 K and 1073 K at 1 K/s [81]. These cycles tended to melt surviving nuclei due to cumulated times of annealing at 1873 K equal to the cycle number multiplied by 300 s [90]. The maximum undercooling was $(\Delta T) = 328 \pm 6$ K. The annealing temperature was too weak compared to $T_{n+} = T_m \times (1 + \theta_{n+})$. Many cycling cannot fully replace an annealing above T_{n+} because there is a first-order phase transition due to the formation of colloids [1]. The minimum value of θ_{n+} is 0.0805 in Table 1 and $T_{n+} = 1910$ K is 37 K higher than the annealing temperature 1873 K. The specific heat C_p of Co crystals is constant from 1440 K to $T_m = 1768$ K and equal to 40.6 J/K/mole [91] (p. 60). The solid fraction formed by recalescence was proportional to the temperature rising and the maximum undercooling was expected to be $(\Delta T) = H_m/C_p = 399$ K instead of 328 K [87]. All the melt was crystallized here. The missing enthalpy represented a fraction equal to 0.178 ± 0.015 of that of melting 16190 J/mole. The reduced temperature θ_{n+} was equal to 0.21655 corresponding to the singular coefficients sum ($0.14490 + 0.07368$) given in Table 2 for Co. The temperature rising after crystallization at 1440 K, and being much weaker than T_m , was not suitable because it was due to non-adiabaticity of the processing [81]. Two peaks of recalescence characterized by temperature rising (ΔT) were observed. The first one in Figure 12 would correspond to the first glacial phase formation through a first-order transition inducing the second peak of full crystallization after an incubation time. The first peak corresponded to two values of $(\Delta T) = 23$ and 91 K for $B = 12$ Tesla and $B = 0$ representing 5.76 and 22.8% of the melting heat. The values of θ_{n+} were 0.0623 instead of 0.0805 and 0.26147 in good agreement with $0.26163 = 0.0805 + 0.18113$ in Table 1.

The conclusions of this chapter are: (i) the full crystallization of liquid elements can occur with reduced entropy and enthalpy at temperatures weaker than T_m in glass-forming melts after heating the material from the glassy state or in the presence of a glacial phase resulting from a high undercooling rate (ii) enthalpy and entropy reductions are also expected for crystallization of quenched glass-forming melts at the well-known temperature called $T_X < T_m$ [92] which could reveal the existence of a second melting temperature at T_{n+} . This crystallization at T_X results from the initial formation of glacial phases by homogeneous nucleation in one or few steps. Two crystallization processes have already been observed above T_g in salol and triphenylethene leading to the same crystal phase with the first one attributed to homogeneous-nucleation-based crystallization at temperatures weaker than T_m [93,94]. Early crystallization following high undercooling shows that the enthalpies of crystallization and melting are reduced. Experiments above

T_m to detect the value of T_{n+} and the recovered enthalpy and entropy at this temperature after early crystallization below T_m are necessary to confirm these proposals.

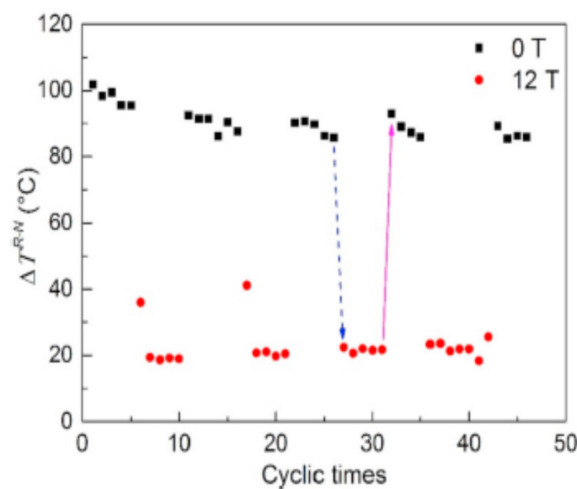


Figure 12. First peak of recalescence: Undercooling (ΔT) of Co at different cycling times under different magnetic fields $B = 0$ and $B = 12$ Tesla. Reprinted with permission from [81]. Copyright 2019 Elsevier.

10. Thermodynamics of Configurons

Configurons are broken chemical bonds in condensed materials [7–12]. In crystalline materials, the configurons are highly mobile and their condensation causes the arrest of temperature at the melting point T_m whereas, in amorphous substances, they move with difficulties and therefore the glass-liquid transition occurs at the glass transition temperature T_g typically as a second order phase transformation. Following the configuron percolation theory (CPT) [7–12], the melting of a material occurs when the percolation via configurons occurs. Therefore, the melting temperature of a material (either T_g for amorphous or T_m for crystalline substances) is:

$$T_m = H_d / (S_d + R \ln[(1 - f_c) / f_c]) \quad (13)$$

where H_d is the enthalpy and S_d is the entropy of formation of configurons, R is the absolute gas constant and f_c is the percolation threshold which is taken at low heating rates as the Scher and Zallen invariant $f_c = 0.15$ [7–12]. The second melting temperature T_{n+} that the CPT treats as percolation via unbroken chemical bonds is:

$$T_{n+} = H_d / (S_d - R \ln[(1 - f_c) / f_c]) \quad (14)$$

Taking the ratios

$$\frac{T_{n+}}{T_m} = \left\{ S_d + R \ln \left[\frac{1 - f_c}{f_c} \right] \right\} / \left\{ S_d - R \ln \left[\frac{1 - f_c}{f_c} \right] \right\} \quad (15)$$

we can find the entropies of configurons in metallic elements as

$$S_d = R \ln \left[\frac{1 - f_c}{f_c} \right] \left[\frac{T_{n+} / T_m + 1}{T_{n+} / T_m - 1} \right] \quad (16)$$

Thereafter we can calculate the enthalpies of elements as

$$H_d = T_m (S_d + R \ln[(1 - f_c) / f_c]). \quad (17)$$

Table 5 gives numerical data of configuron entropies and enthalpies and enthalpies H and entropies S of melting as calculated, decreasing with T_{n+}/T_m .

Table 5. Thermodynamic data for configurons in metals. T_m the melting temperature in Kelvin; T_{n+}/T_m the second melting temperature divided by T_m ; S_d the configuron entropy in units of $R = 8.34$ J; H_d the configuron enthalpy in KJ/mol; $S/S_m = H/H_m$ the ratio of the second melting entropy and S_m equal to the ratio of the second melting enthalpy and H_m .

Metal	T_m , K	T_{n+}/T_m	S_d (in Units of R)	H_d , KJ/mol	$S/S_m = H/H_m$
Co	1768	1.0805	44.83	686.60	0.925
Zr	2125	1.11896	30.90	578.32	0.894
Ag	1235	1.12648	29.16	318.25	0.888
Fe	1811	1.21866	17.60	292.03	0.821
Ta	3288	1.29050	13.68	422.60	0.775
Re	3458	1.318	12.64	414.67	0.759
Cu	1358	1.35413	11.53	140.19	0.738

11. A New Panorama for Melting and Solidification

A melting heat H_m is measured by melting a solid element at T_m . The melting entropy is $S_m = H_m/T_m$. Various thermal histories can lead to at least three liquid states: the first one has a complementary exothermic melting temperature at T_{n+} , the second one has a complementary endothermic melting temperature at T_{n+} and the third one is homogeneous above T_{n+} . The reduced temperature θ_{n+} is multiple and equal to singular values of enthalpy coefficients which are predicted by glacial phase formation leading to more numerous liquid states having various enthalpy differences with that of homogeneous liquid above θ_{n+} . High heating rates rise the temperature of full melting up to T_{n+} which can attain and even exceed $1.47 T_m$ for liquids having high enthalpy excesses. The liquid states can be more than three depending in the number of singular enthalpies of glacial phases.

These phenomena of new liquid formation are characterized by variations of the enthalpy H_m and the entropy S_m accompanying melting and crystallization. The melting temperature rising is not only due to high heating rates and is observable in highly undercooled systems close to crystallization. Melting temperature increase at high heating rate observed in MD simulations cannot be due to overheating of the solid phase because the classical nucleation equation predicts a full melting at T_m without residual crystals in the melt [95]. Our description is based on the melting of superheated glassy phase at the temperature T_{n+} having an enthalpy of melting equal to that of crystalline phase.

The existence of temperatures T_{n+} in glass-forming melts was recently confirmed at heating rates of about 0.5 K/s [1,51–68]. They are due to the formation of antibonds increasing the liquid enthalpy above T_m up to T_{n+} or bonds decreasing the liquid enthalpy in the interval (T_m, T_{n+}) . Recent review confirms the existence of liquid-liquid structure transitions in melts above T_m and their impact on the following microstructure and properties after solidification [96]. A liquid-liquid transition is observed at 1575 ± 6 K in $\text{Co}_{81.5}\text{B}_{18.5}$ eutectics above a melting temperature $T_m = 1406$ K which could correspond to $T_g = 869 \pm 19$ K in this fragile liquid [97].

The liquid microstructure is changed by cooling the melt through T_{n+} which is induced by a first-order transition from homogeneous liquid to various colloids of various compositions [54,66,68]. The colloids result from the formation of melted superatoms containing magic atom numbers discontinuously varying shell by shell with temperature [98,99]. At the temperature T_{n+} , the Gibbs free energy change during cooling, favorizing the colloids formation [1], is higher than that of a continuous variation, enhanced by nucleation of bonds versus time at temperatures weaker than T_{n+} , building clusters-bound colloids. These colloids contain more and more bonds and give rise to crystallization at T_m at low cooling rate or to glassy phase after quenching to escape from crystallization. These formations of colloids of various compositions were observed many years ago for eutectic and off-eutectic compositions [54,100,101].

12. Conclusions

Recent molecular dynamics simulations observed second melting temperatures T_{n+} of pure elements varying from 1.11896 T_m for zirconium to 1.35413 T_m for copper applying

very high heating rates. The non-classical model of homogeneous nucleation (NCHN model) predicted these temperatures as melting temperatures of glassy glacial phases formed by homogeneous nucleation at temperatures T_{nG} weaker than T_{n+} . These nucleation temperatures T_{nG} cannot be higher than $1.2931 T_m$. A universal law of T_{n+}/T_m versus (T_{nG}/T_m) was obtained for all liquid elements with a Lindemann coefficient weaker than 0.137.

These glacial phases had singular constant values of enthalpy up to their upper glass transitions equal to T_{n+} . The NCHN model needed singular values of enthalpy to be applied at well-defined temperatures. They corresponded to singular values of the enthalpy coefficient $\Delta\varepsilon_{lg}(\theta)$ of a new phase called Phase 3 or configuron phase. These percolation threshold values must be singular to represent various organizations of elementary bricks in a glass.

The NCHN model agreed with existing MD simulations using recent values of the Lindemann coefficient of elements presented in the columns of Figure 1 to predict the value of T_g . Consequently, this figure and the universal law could be used to control MD simulations of other elements.

Phase 3 was induced by a first-order transition at T_{nG} by cooling and was accompanied by a second-order phase transition during reheating as predicted by formation of percolation threshold of broken bonds named configurons.

Second melting temperatures T_{n+} have been already observed in several glass-forming melts accompanied by exothermic or endothermic latent heats at lower heating rates. They corresponded to the melting of antibonds or bonds induced by thermal history depending on cooling and heating rates from the homogeneous liquid state down to the glassy phase and from the glassy phase to high temperatures.

The existence of temperatures T_{n+} in liquid elements has for consequence entropy and enthalpy reductions for melting. These effects are observed in all situations already described. They need to be confirmed by early crystallization of highly undercooled melts having previously undergone a glacial phase transition. We have looked at two experiments: (i) the free fall solidification of Tantalum and Rhenium droplets with two recalescence peaks and (ii) those of undercooled cobalt in a high magnetic field $B = 12$ Tesla and $B = 0$. These experiments confirmed these reductions. Observations of T_{n+} above T_m are expected after observing these crystallizations at T_x below T_m .

The NCHN and configuron models successfully predicted liquid–glass and liquid–liquid transformations in multicomponent glass-forming melts. These predictions are possible when the glass transition temperature T_g and the melting temperatures T_m are sufficiently precise to be able to determine the singular values of Phase 3 enthalpy. The universal law relating the nucleation temperatures T_{nG} of glacial phases and the second melting temperatures T_{n+} in multicomponent alloys could be the same to that of pure elements.

Author Contributions: Conceptualization, R.F.T. and M.I.O.; methodology, R.F.T.; software, R.F.T.; validation, R.F.T. and M.I.O.; formal analysis, R.F.T.; investigation, R.F.T.; resources, R.F.T. and M.I.O.; data curation, R.F.T.; writing—original draft preparation, R.F.T.; writing—review and editing, R.F.T. and M.I.O.; visualization, R.F.T.; supervision, R.F.T. and M.I.O. All authors have read and agreed to the published version of the manuscript.

Funding: This research received no external funding.

Institutional Review Board Statement: Not Applicable.

Informed Consent Statement: Not applicable.

Data Availability Statement: Data supporting reported results are available from the authors.

Conflicts of Interest: The authors declare no conflict of interest.

References

1. Tournier, R.F.; Ojovan, M.I. Building and breaking bonds by homogenous nucleation in glass-forming melts leading to three liquid states. *Materials* **2021**, *14*, 2287. [[CrossRef](#)]
2. Tournier, R.F. First-order transitions in glasses and melts induced by solid superclusters nucleated by homogeneous nucleation instead of surface melting. *Chem. Phys.* **2019**, *524*, 40–54. [[CrossRef](#)]
3. Wang, L.-M.; Borick, S.; Angell, C.A. An electrospray technique for hyperquenched glass calorimetry studies: Propylene glycol and di-n-butylphthalate. *J. Non-Cryst. Solids* **2007**, *353*, 3829–3837. [[CrossRef](#)]
4. Hornboll, L.; Yue, Y. Enthalpy relaxation in hyperquenched glasses of different fragility. *J. Non-Cryst. Solids* **2008**, *354*, 1832–1870. [[CrossRef](#)]
5. Inoue, A.; Zhang, T.; Masumoto, T. The structural relaxation and glass transition of La-Al-Ni and Zr-Al-Cu amorphous alloys with a significant supercooled liquid region. *J. Non-Cryst. Solids* **1992**, *150*, 396. [[CrossRef](#)]
6. Hu, L.; Zhang, C.; Yue, Y. Thermodynamic anomaly of the sub- T_g relaxation in hyperquenched metallic glasses. *J. Chem. Phys.* **2013**, *138*, 174508. [[CrossRef](#)] [[PubMed](#)]
7. Ozhovan, M.I. Topological characteristics of bonds in SiO₂ and GeO₂ oxide systems at glass-liquid transition. *J. Exp. Theor. Phys.* **2006**, *103*, 819–829. [[CrossRef](#)]
8. Ojovan, M.I.; Travis, K.P.; Hand, R.J. Thermodynamic parameters of bonds in glassy materials from viscosity temperature relationships. *J. Phys. Cond. Matter.* **2007**, *19*, 415107. [[CrossRef](#)]
9. Ojovan, M.I.; Lee, W.E. Connectivity and glass transition in disordered oxide systems. *J. Non-Cryst. Solids* **2010**, *356*, 2534–2540. [[CrossRef](#)]
10. Ojovan, M.I. Ordering and structural changes at the glass-liquid transition. *J. Non-Cryst. Solids* **2013**, *382*, 79. [[CrossRef](#)]
11. Ojovan, M.I.; Louzguine-Luzgin, D.V. Revealing Structural Changes at Glass Transition via Radial Distribution Functions. *Phys. B* **2020**, *124*, 3186–3194. [[CrossRef](#)]
12. Ojovan, M.I.; Tournier, R.F. On structural rearrangements in amorphous silica at the glass transition. *Materials* **2021**, *14*, 5235. [[CrossRef](#)]
13. Kearns, K.L.; Whiteker, K.R.; Ediger, M.D.; Huth, H.; Schick, C. Observation of low heat capacities for vapor-deposited glasses of indomethacin as determined by AC nanocalorimetry. *J. Chem. Phys.* **2010**, *133*, 014702. [[CrossRef](#)] [[PubMed](#)]
14. Kearns, K.L.; Swallen, S.F.; Ediger, M.D.; Wu, T.; Sun, Y.; Yu, L. Hiking down the energy landscape: Progress toward the Kauzmann temperature via vapor deposition. *J. Phys. Chem. B.* **2008**, *112*, 4934–4942. [[CrossRef](#)] [[PubMed](#)]
15. Kearns, K.L.; Swallen, S.F.; Ediger, M.D.; Wu, T.; Yu, L. Influence of substrate temperature on the stability of glasses prepared by vapor deposition. *J. Chem. Phys.* **2007**, *127*, 154702. [[CrossRef](#)]
16. Whiteker, K.R.; Scifo, D.J.; Ediger, M.D.; Ahrenberg, M.; Schick, C. High stable glasses of cis-decalin and cis/trans-decalin mixtures. *J. Phys. Chem.* **2013**, *117*, 12724–12733. [[CrossRef](#)]
17. Whiteker, K.R.; Tylinski, M.; Ahrenberg, M.; Schick, C.; Ediger, M.D. Kinetic stability and heat capacity of vapor-deposited glass of o-terphenyl. *J. Chem. Phys.* **2015**, *143*, 084511. [[CrossRef](#)]
18. Ahrenberg, M.; Chua, Y.Z.; Whitaker, R.; Huth, H.; Ediger, M.D.; Schick, C. In situ investigation of vapor-deposited glasses of toluene and ethylbenzene via alternating current chip-nanocalorimetry. *J. Chem. Phys.* **2013**, *138*, 024501. [[CrossRef](#)]
19. Tylinski, M.; Chua, Y.Z.; Beasley, M.S.; Ediger, M.D. Vapor-deposited alcohol glasses reveal a wide-range of kinetic stability. *J. Chem. Phys.* **2016**, *145*, 174506. [[CrossRef](#)]
20. Ramos, S.L.; Oguni, M.; Ishii, K.; Nakayama, H. Character of devitrification, viewed from enthalpic paths, of the vapor-deposited ethylbenzene glasses. *J. Phys. Chem. B.* **2011**, *115*, 14327–14332. [[CrossRef](#)]
21. Leon-Gutierrez, E.; Sepulveda, A.; Garcia, G.; Clavaguera-Mora, M.T.; Rodriguez-Vieja, J. Stability of thin film glasses of toluene and ethylbenzene formed by vapor deposition: An in-situ nanocalorimetric study. *Phys. Chem. Chem. Phys.* **2010**, *12*, 14693–14698. [[CrossRef](#)]
22. Yu, H.-B.; Luo, Y.; Samwer, K. Ultrastable metallic glass. *Adv. Mater.* **2013**, *25*, 5904–5908. [[CrossRef](#)]
23. Wang, J.Q.; Shen, Y.; Perepezko, J.H.; Ediger, M.D. Increasing the kinetic stability of bulk metallic glasses. *Acta Mater.* **2016**, *104*, 25–32. [[CrossRef](#)]
24. Beasley, M.S.; Tylinski, M.; Chua, Y.Z.; Schick, C.; Ediger, M.D. Glasses of three alkyl phosphates show a range of kinetic stabilities when prepared by physical vapor deposition. *J. Chem. Phys.* **2018**, *148*, 174503. [[CrossRef](#)]
25. Chua, Y.Z.; Ahrenberg, M.; Tylinski, M.; Ediger, M.D.; Schick, C. How much time is needed to form a kinetically stable glass? Ac calorimetric study of vapor-deposited glasses of ethylcyclohexane. *J. Chem. Phys.* **2015**, *142*, 054506. [[CrossRef](#)] [[PubMed](#)]
26. Kivelson, D.; Kivelson, S.A.; Zhao, X.; Nussinov, Z.; Tarjus, G. A thermodynamic theory of supercooled liquids. *Phys. A* **1995**, *219*, 27–38. [[CrossRef](#)]
27. Ha, A.; Cohen, I.; Zhao, X.; Lee, M.; Kivelson, D. Supercooled liquids and polyamorphism. *J. Phys. Chem. Lett.* **1996**, *100*, 1–4. [[CrossRef](#)]
28. Kurita, R.; Tanaka, H. On the abundance and general nature of the liquid-liquid phase transition in molecular systems. *J. Phys. Condens. Matter.* **2005**, *17*, L293–L302. [[CrossRef](#)]
29. Kobayashi, M.; Tanaka, H. The reversibility and first-order nature of liquid-liquid transition in a molecular liquid. *Nat. Comm.* **2016**, *7*, 13438. [[CrossRef](#)]

30. Zhu, M.; Wang, J.-Q.; Perepezko, J.H.; Yu, L. Possible existence of two amorphous phases of D-Mannitol related by a first-order transition. *J. Chem. Phys.* **2015**, *142*, 244504. [[CrossRef](#)]
31. Tournier, R.F. Homogeneous nucleation of phase transformations in supercooled water. *Phys. B* **2020**, *579*, 411895. [[CrossRef](#)]
32. Kurtuldu, G.; Shamlaye, K.F.; Löffler, J. Metastable quasi-crystal-induced nucleation in a bulk glass-forming melt. *Proc. Natl. Acad. Sci. USA* **2018**, *115*, 6123–6128. [[CrossRef](#)] [[PubMed](#)]
33. Tournier, R.F.; Ojovan, M.I. Undercooled Phase Behind the Glass Phase with Superheated Medium-Range Order above Glass Transition Temperature. *Physica B* **2021**, *602*, 412542. [[CrossRef](#)]
34. Tournier, R.F.; Ojovan, M.I. Dewetting Temperatures of Prefrozen and Grafted Layers in Ultrathin Films Viewed as Melt-Memory Effects. *Physica B* **2021**, *611*, 412796. [[CrossRef](#)]
35. Shen, J.; Lu, Z.; Wang, J.Q.; Lan, S.; Zhang, F.; Chen, M.W.; Wang, X.L.; Wen, P.; Sun, Y.H.; Bai, H.Y.; et al. Metallic glacial glass formation by a first-order liquid-liquid transition. *J. Phys. Chem. Lett.* **2020**, *11*, 6718–6723. [[CrossRef](#)] [[PubMed](#)]
36. Tournier, R.F. Presence of intrinsic growth nuclei in overheated and undercooled liquid elements. *Physica B* **2007**, *392*, 79–91. [[CrossRef](#)]
37. Tournier, R.F. Crystal growth nucleation and Fermi energy equalization of intrinsic spherical nuclei in glass-forming melts. *Sci. Technol. Adv. Mater.* **2009**, *10*, 014617. [[CrossRef](#)]
38. Tournier, R.F. Thermodynamic origin of the vitreous transition. *Materials* **2011**, *4*, 869–892. [[CrossRef](#)]
39. Tournier, R.F. Thermodynamic and kinetic origin of the vitreous transition. *Intermetallics* **2012**, *30*, 104–110. [[CrossRef](#)]
40. Tournier, R.F. Fragile-to-fragile liquid transition at T_g and stable-glass phase nucleation rate maximum at the Kauzmann temperature. *Physica B* **2014**, *454*, 253–271. [[CrossRef](#)]
41. Tournier, R.F. Predicting glass-to-glass and liquid-to-liquid phase transitions in supercooled water using non-classical nucleation theory. *Chem. Phys.* **2018**, *500*, 45–53. [[CrossRef](#)]
42. Tournier, R.F. Amorphous ices. In *Encyclopedia of Glass Science, Technology, History, and Culture*; Richet, P., Ed.; Wiley & Sons: Hoboken, NJ, USA, 2021; Volume 1, p. 3.14.
43. Angell, C.A.; Rao, K.J. Configurational excitations in condensed matter and the “bond lattice”. Model for the liquid-glass transition. *J. Chem. Phys.* **1972**, *57*, 470–481. [[CrossRef](#)]
44. Kuchemann, S.; Gibbins, G.; Corkerton, J.; Brug, E.; Ruebsam, J.; Samwer, K. From ultrafast to slow: Heating rate dependence of the glass transition temperature in metallic systems. *Phil. Mag. Lett.* **2016**, *96*, 454–460. [[CrossRef](#)]
45. An, Q.; Johnson, W.L.; Samwer, K.; Corona, S.L.; Goddard, W.A., III. First-order transition in liquid Ag to the heterogeneous G-Phase. *J. Phys. Chem. Lett.* **2020**, *11*, 632–645. [[CrossRef](#)]
46. An, Q.; Johnson, W.L.; Samwer, K.; Corona, S.L.; Goddard, W.A., III. Formation of two glass phases in binary Cu-Ag liquid. *Acta Mater.* **2020**, *195*, 274–281. [[CrossRef](#)]
47. Daeges, J.; Gleiter, H.; Perepezko, J.H. Superheating of metal crystals. *Phys. Lett. A.* **1986**, *119*, 79–82. [[CrossRef](#)]
48. Lu, K.; Sheng, H.; Jin, Z. Melting and superheating of crystals. *Chin. J. Mater. Res.* **1997**, *11*, 658–665.
49. Zhang, D.L.; Cantor, B. Melting behaviour of In and Pb particles embedded in an Al Matrix. *Acta Metall. Mater.* **1991**, *39*, 1595–1602. [[CrossRef](#)]
50. Lu, K.; Li, Y. Homogeneous nucleation catastrophe as a kinetic stability limit for superheated crystal. *Phys. Rev. Lett.* **1998**, *80*, 4474–4477. [[CrossRef](#)]
51. Tournier, R.F. Glass phase and other multiple liquid-to-liquid transitions resulting from two-liquid competition. *Chem. Phys. Lett.* **2016**, *665*, 64–70. [[CrossRef](#)]
52. Li, J.J.Z.; Rhim, W.K.; Zeng, X.R.; Samwer, K.; Johnson, W.L. Evidence for a liquid-liquid phase transition in metallic fluid observed by electrostatic levitation. *Acta Mater.* **2011**, *59*, 2166–2171. [[CrossRef](#)]
53. Hu, Q.; Sheng, H.C.; Fu, M.W.; Zeng, X.R. Influence of melt temperature on the Invar effect in $(\text{Fe}_{71.2}\text{B}_{0.24}\text{Y}_{4.8})_{96}\text{Nb}_4$ bulk metallic glasses. *J. Mater. Sci.* **2019**, *48*, 6900–6906.
54. Popel, P.S.; Sidorov, V.E. Microheterogeneity of liquid metallic solutions and its influence on the structure and properties of rapidly quenched alloys. *Mater. Sci. Eng.* **1997**, *226–228*, 237–244. [[CrossRef](#)]
55. Lan, S.; Blodgett, M.; Kelton, K.F. Structural crossover in a supercooled metallic liquid and the link to a liquid-to-liquid phase transition. *Appl. Phys. Lett.* **2016**, *108*, 211907. [[CrossRef](#)]
56. Mukherjee, S.; Zhou, Z.; Schroers, J.; Johnson, W.L.; Rhim, W.K. Overheating threshold and its effect on time-temperature-transformation diagrams of zirconium based bulk metallic glasses. *Appl. Phys. Lett.* **2004**, *84*, 5010–5012. [[CrossRef](#)]
57. Busch, R.; Kim, H.J.; Johnson, W.L. Thermodynamic and kinetics of the undercooled liquid and the glass transition of the $\text{Zr}_{41.2}\text{Ti}_{13.6}\text{Cu}_{12.5}\text{Ni}_{10.0}\text{Be}_{22.5}$ alloy. *J. Appl. Phys.* **1995**, *77*, 4039–4043. [[CrossRef](#)]
58. He, Y.; Li, J.; Wang, J.; Kou, H.; Beaunon, E. Liquid-liquid structure transition and nucleation in undercooled Co-B eutectic alloys. *Appl. Phys. A.* **2017**, *123*, 391. [[CrossRef](#)]
59. Yang, B.; Perepezko, J.H.; Schmelzer, J.W.P.; GaO, Y.; Schick, C. Dependence of crystal nucleation on prior liquid overheating by differential fast scanning calorimetry. *J. Chem. Phys.* **2014**, *140*, 104513. [[CrossRef](#)]
60. Wei, S.; Yang, F.; Bednarcik, J.; Kaban, I.; Shuleshova, O.; Meyer, A.; Busch, R. Liquid-liquid transition in a strong bulk metallic glass-forming liquid. *Nat. Commun.* **2013**, *4*, 2083. [[CrossRef](#)]
61. Way, C.; Wadhwa, P.; Busch, R. The influence of shear rate and temperature on the viscosity and fragility of the $\text{Zr}_{41.2}\text{Ti}_{13.6}\text{Cu}_{12.5}\text{Ni}_{10.0}\text{Be}_{22.5}$ metallic-glass-forming liquid. *Acta Mater.* **2007**, *55*, 2977–2983. [[CrossRef](#)]

62. Jiang, H.-R.; Bochtler, B.; Riegler, S.S.; Wei, X.-S.; Neuber, N.; Frey, M.; Gallino, I.; Busch, R.; Shen, J. Thermodynamic and kinetic studies of the Cu-Zr-Al(-Sn) bulk metallic glasses. *J. All. Comp.* **2020**, *844*, 156126. [\[CrossRef\]](#)
63. Kim, Y.H.; Kiraga, K.; Inoue, A.; Masumoto, T.; Jo, H.H. Crystallization and high mechanical strength of Al-based amorphous alloys. *Mater. Trans.* **1994**, *35*, 293–302. [\[CrossRef\]](#)
64. Dahlborg, U.; Calvo-Dahlborg, M.; Popel, P.S.; Sidorov, V.R. Structure and properties of some glass-forming liquid alloys. *Eur. Phys. J.* **2000**, *B14*, 639–648. [\[CrossRef\]](#)
65. Yue, Y. Experimental evidence for the existence of an ordered structure in a silicate liquid above its liquidus temperature. *J. Non-Cryst. Solids* **2004**, *345–346*, 523–527. [\[CrossRef\]](#)
66. Chen, E.-Y.; Peng, S.-X.; Peng, L.; Michiel, M.D.; Vaughan, G.B.M.; Yu, Y.; Yu, H.-B.; Ruta, B.; Wei, S.; Liu, L. Glass-forming ability correlated with the liquid-liquid transition in Pd_{42.5}Ni_{42.5}P₁₅ alloy. *Scripta Mater.* **2021**, *193*, 117–121. [\[CrossRef\]](#)
67. Lan, S.; Ren, Y.; Wei, X.Y.; Wang, B.; Gilbert, E.P.; Shibayama, T.; Watanabe, S.; Ohnuma, M.; Wang, X.-L. Hidden amorphous phase and reentrant supercooled liquid in Pd-Ni-P metallic glass. *Nat. Commun.* **2017**, *8*, 14679. [\[CrossRef\]](#)
68. Xu, W.; Sandor, M.T.; Yu, Y.; Ke, H.-B.; Zhang, H.P.; Li, M.-Z.; Wang, W.-H.; Liu, L.; Wu, Y. Evidence of liquid-liquid transition in glass-forming La₅₀Al₃₅Ni₁₅ melt above liquidus temperature. *Nat. Commun.* **2015**, *6*, 7696. [\[CrossRef\]](#)
69. Zeng, Y.Q.; Yu, J.S.; Tian, Y.; Hirata, A.; Fujita, T.; Zhang, X.H.; Nishiyama, N.; Kato, H.; Jiang, J.Q.; Inoue, A.; et al. Improving glass forming ability of off-eutectic metallic glass formers by manipulating primary crystallization reactions. *Acta Mater.* **2020**, *200*, 710–719. [\[CrossRef\]](#)
70. Tournier, R.F.; Ojovan, M.I. Comments about a recent publication entitled "Improving glass forming ability of off-eutectic metallic glass formers by manipulating primary crystallization reactions". *Scripta Mater.* **2021**. under publication. [\[CrossRef\]](#)
71. Zeng, Y.Q.; Yu, J.S.; Tian, Y.; Hirata, A.; Fujita, T.; Zhang, X.H.; Nishiyama, N.; Kato, H.; Jiang, J.Q.; Inoue, A.; et al. Response to the commentary by Robert Tournier and Michael Ojovan on our publication entitled "Improving glass forming". *Scripta Mater.* **2021**. under publication. [\[CrossRef\]](#)
72. Tournier, R.F. Lindemann's rule applied to the melting of crystals and ultra-stable glasses. *Chem. Phys. Lett.* **2016**, *651*, 198–202, Erratum in **2017**, *675*, 174. [\[CrossRef\]](#)
73. Bossy, J.; Hansen, T.; Glyde, H.R. Amorphous solid Helium in porous melts. *Phys. Rev. B* **2010**, *81*, 184507. [\[CrossRef\]](#)
74. Bera, S.; Maloney, J.; Mulders, N.; Cheng, Z.G.; Chan, M.H.W.; Burns, C.A.; Zhang, S. Pressure-dependent phase transformation of solid helium confined with a nanoporous material. *Phys. Rev. B* **2013**, *88*, 054512. [\[CrossRef\]](#)
75. Tournier, R.F.; Bossy, J. ⁴He glass phase: A model for liquid elements. *Chem. Phys. Lett.* **2016**, *658*, 282–286. [\[CrossRef\]](#)
76. Tournier, R.F. Validation of non-classical homogeneous nucleation model for G-glass and L-glass formations in liquid elements with recent molecular dynamics simulations. *Scripta Mater.* **2021**, *199*, 113859. [\[CrossRef\]](#)
77. Vopson, M.M.; Rugers, N.; Hepburn, I. The generalized Lindemann Melting coefficient. *Sol. State Commun.* **2020**, *318*, 113977. [\[CrossRef\]](#)
78. Bazlov, A.I.; Louzguine-Luzguin, D.V. Crystallization of FCC and BCC liquid metals studied by molecular dynamics simulation. *Metals* **2020**, *10*, 1532.
79. Becker, S.; Devijver, E.; Molinier, R.; Jakse, N. Glass-forming ability of elemental zirconium. *Phys. Rev. B* **2020**, *102*, 104205. [\[CrossRef\]](#)
80. Cortella, L.; Vinet, B.; Desre, P.J.; Pasturel, A.; Paxton, A.T.; Van Schilfgaarde, M. Evidences of transition metastable phases in refractory metals solidified from highly undercooled liquids in a droplet. *Phys. Rev. Lett.* **1993**, *70*, 1469–1472. [\[CrossRef\]](#)
81. Wang, J.; He, Y.; Li, J.; Li, C.; Kou, H.; Zhang, P.; Beaunon, E. Nucleation of supercooled Co melts under a high magnetic field. *Mater. Chem. Phys.* **2019**, *225*, 133–136. [\[CrossRef\]](#)
82. Shephard, J.J.; Salzman, C.G. Molecular reorientation dynamics govern the glass transition of the amorphous state. *J. Phys. Chem. Lett.* **2016**, *7*, 2181–2185. [\[CrossRef\]](#)
83. Shephard, J.J.; Ling, S.; Sosso, G.C.; Michalides, A.; Slater, B.; Salzman, C.G. High-density amorphous ice simply-derailed state along the ice 1 to ice IV pathway. *J. Phys. Chem. Lett.* **2017**, *8*, 1645–1650. [\[CrossRef\]](#) [\[PubMed\]](#)
84. Zhong, L.; Wang, J.; Sheng, H.; Zhang, Z.; Mao, S.X. Formation of monoatomic metallic glasses through ultrafast liquid quenching. *Nature* **2014**, *512*, 177. [\[CrossRef\]](#)
85. Louzguine-Luzguin, D.V.; Belosludov, R.; Saito, M.; Kawazoe, Y.; Inoue, A. Glass transition behavior of Ni: Calculation, prediction, and experiment. *J. Appl. Phys.* **2008**, *104*, 123529. [\[CrossRef\]](#)
86. Louzguine-Luzgin, D.V.; Miyama, M.; Nishio, N.; Tsarkov, A.A.; Greer, A.L. Vitrification and nanocrystallization of pure liquid Ni studied using molecular-dynamics simulation. *J. Chem. Phys.* **2019**, *151*, 124502. [\[CrossRef\]](#)
87. Herlach, D.M. Non-equilibrium solidification of undercooled metallic melts. *Mater. Sci. Eng.* **1994**, *R12*, 177–272. [\[CrossRef\]](#)
88. Stewart, G.R. Measurement of low-temperature specific heat. *Rev. Sci. Instrum.* **1983**, *54*, 1–11. [\[CrossRef\]](#)
89. Taylor, R.E.; Finch, R.A. The Specific Heats and Resistivities of Molybdenum, Tantalum, and Rhenium from Low to High Temperatures. s.l.: Standard Distribution Lists for Unclassified Scientific and Technical Reports. In Proceedings of the Atomic International, Canoga Park, CA, USA, 15 December 1960; TID-4500 (16th Ed.); 1960; pp. 1–37.
90. Tournier, R.F. Crystallization of supercooled liquid elements induced by superclusters containing magic atom numbers. *Metals* **2014**, *4*, 359–387. [\[CrossRef\]](#)
91. Thurnay, K. *Properties of Transition Metals*; Forschungszentrum Karlsruhe: Karlsruhe, Germany, 1998. [\[CrossRef\]](#)
92. Inoue, A. Stabilization of metallic supercooled liquid and bulk amorphous alloys. *Acta Mater.* **2000**, *48*, 279–306. [\[CrossRef\]](#)

93. Hikima, T.; Okamoto, N.; Hanaya, M.; Oguni, M. Calorimetric study of triphenylethene: Observation of homogeneous-nucleation-based crystallization. *J. Chem. Therm.* **1998**, *30*, 509–523. [[CrossRef](#)]
94. Hikima, T.; Hanaya, M.; Oguni, M. Discovery of a potentially homogeneous-nucleation-based crystallization around the glass transition temperature in Salol. *Solid State Comm.* **1995**, *93*, 713–717. [[CrossRef](#)]
95. Kelton, K.F. Crystal nucleation in liquids and glasses. *Solid State Phys.* **1991**, *45*, 75–177.
96. He, Y.-X.; Li, J.-S.; Wang, J.; Beaugnon, E. Liquid-liquid structure transition in metallic melt and its impact on solidification: A review. [ed.] Elsevier. *Trans. Nonferr. Met. Soc. China* **2020**, *30*, 2293–2310. [[CrossRef](#)]
97. He, Y.; Li, J.; Li, L.; Wang, J.; Yildiz, E.; Beaugnon, E. Composition dependent characteristic transition temperatures of Co-B melts. *J. Non-Cryst. Solids* **2019**, *522*, 119583. [[CrossRef](#)]
98. Tlahuice-Flores, A.; Munoz-Castro, A. Bonding and properties of superatoms. Analogs to atoms and molecules and related concepts from superatomic clusters. *J. Quantum Chem.* **2019**, *119*, e25756. [[CrossRef](#)]
99. Kuzmin, V.I.; Tytik, D.I.; Belashchenko, G.K.; Sirenko, A.N. Structure of silver clusters with magic numbers of atoms by data of molecular dynamics. *Colloid J.* **2008**, *70*, 284–296. [[CrossRef](#)]
100. Popel, P.S.; Chikova, O.A.; Matveev, V.M. Metastable colloidal states of liquid metallic solutions. *High Temp. Mater. Proc.* **1995**, *4*, 219–233. [[CrossRef](#)]
101. Popel, P.S.; Dahlborg, U.; Calvo-Dahlborg, M. On the existence of metastable microheterogeneities in metallic melts. *IOP Conf. Ser. Mater.Sci. Eng.* **2017**, *192*, 012012. [[CrossRef](#)]